Carrier transport in methylammonium lead iodide perovskite single crystals studied by dark current, steady state and transient photocurrent measurements

Reynolds, Stephen; Houghton, Anthony; Keeble, David

Published in:
Journal of Physics: Conference Series

DOI:
10.1088/1742-6596/1186/1/012035

Publication date:
2019

Carrier transport in methylammonium lead iodide perovskite single crystals studied by dark current, steady state and transient photocurrent measurements

IOP Conf. Series: Journal of Physics: Conf. Series **1186** (2019) 012035 doi:10.1088/1742-6596/1186/1/012035

Carrier transport in methylammonium lead iodide perovskite single crystals studied by dark current, steady state and transient photocurrent measurements

S Reynolds[1], A R Houghton[1,2] and D J Keeble[1]

[1] School of Science and Engineering, University of Dundee, Dundee DD1 4HN, UK.
[2] Present address: Department of Chemical Engineering, Imperial College, South Kensington Campus, London SW7 2AZ, UK.

E-mail: s.z.reynolds@dundee.ac.uk

Abstract. Electronic transport properties of methylammonium lead iodide perovskite single crystals prepared by inverse temperature crystallisation have been investigated using dark current, steady state and transient photocurrent measurements. Above 250 K the dark conductivity at electric fields below 100 V/cm is thermally activated, with single activation energy 0.7 eV and magnitude 4×10^{-8} S/cm at 300 K. At higher electric fields, conductivity increases as a power law suggesting space charge limitation. Steady state photoconductivity exhibits a roughly linear dependence on photon flux below 10^{15} $cm^{-2}s^{-1}$ and square root dependence above this, consistent with trap-limited and band-to-band recombination mechanisms respectively. Photocurrent overshoot and undershoot on a timescale of 10-100 s are observed on application and removal of a steady light source. Transient photocurrent measurements with temperature reveal a peak in the localised density of states 0.26 eV into the band gap, with an attempt to escape frequency of 10^{11} s^{-1}. Deeper states are distributed exponentially with characteristic energy 54 meV, decreasing towards mid-gap.

1. Introduction

Over the past decade, methylammonium lead tri-halide perovskite solar cells have maintained a spectacular year-on-year increase in headline photovoltaic conversion efficiency, now surpassing 22% [1, 2], but their tendency to degrade and become unstable on exposure to light, heat and ambient atmosphere is also well-known [3]. The member of this family studied most extensively is *methylammonium lead tri-iodide* $CH_3NH_3PbI_3$, commonly referred to by the acronym MAPI. MAPI has a direct bandgap of 1.5 eV, high optical absorption coefficient, steep absorption edge and good carrier transport properties, and may be solution-processed into solar cell absorber layers.

While thin films are of greater interest for large-area solar cell applications, single crystals generally have the advantage of being less affected by surface phenomena and structural disorder, and enable the intrinsic material properties to be studied more directly. Simple methods of growing single MAPI crystals several cm^2 on a face, of good electronic quality, from solution have been developed, including *inverse temperature crystallisation* (ITC) [4, 5]. This relies upon the fact that crystallisation of product from solutions of precursor compounds is favoured, in certain solvents, at higher temperatures. The choice of solvent also depends upon the solubility of the precursors.

We have carried out a range of measurements on MAPI single crystals grown using ITC. These include thermally-activated dark conductivity, space-charge limited currents, steady-state and switch-

on/switch-off photoconductivity, and short pulse transient photoconductivity (TPC). From this we seek to quantify their electronic transport properties, in particular intrinsic electronic defect density of states (DOS) and its energetic distribution, and to gain insight into why these semiconductors are such promising photovoltaic (PV) absorbers but also show a strong tendency towards instability.

2. Experimental

2.1. Growth of MAPI single crystals

1 mole quantities of PbI_2 (4.61 g) and CH_3NH_3I (1.59 g) precursors were dissolved in 10 ml γ-butyrolactone solvent by magnetic stirring at approximately 60 °C for 30 minutes. A 2 ml portion was then pipetted into a flat bottom screw-top glass vial and placed in a silicone oil bath at 110 °C. Over a period of some three hours, MAPI crystals 1-2 mm in size were formed, and were recovered by passing the liquor through filter paper. To increase their size, the process was repeated using selected crystals with good morphology as seeds, placed in fresh solution. The above procedures were carried out in a fume cupboard under ambient conditions and 20-30% relative humidity.

MAPI crystals exhibit rhombo-hexagonal dodecahedral morphology; examples are shown in figure 1(a). Planar electrical contacts were formed on the upper facet using silver conductive paste, leaving a gap of approximately 0.5 mm, as shown in figure 1(b). This rather crude gap-cell arrangement enables photocurrent measurements to be made by directing light between the contacts. As the thickness of the crystal (in the direction orthogonal to the upper facet) was typically 2 mm, this sample geometry does not conform particularly well to any of the usual approximations. To estimate dark conductivity, the active sample thickness was assumed equal to the contact separation. The crystal was mounted on a ceramic substrate, and placed in a cryostat pumped to 10^{-2} torr over the entire measurement period to minimise contamination. A 6 mm diameter quartz rod was used to transfer light on to the sample.

While MAPI crystals were normally mounted and measured shortly after growth, they could be stored in a dessicator for periods of weeks without significant degradation being visible or electrically detectable. Discarded samples may develop regions of yellow colouration after several days at ambient, associated with an undesirable hydrated form of the material.

2.2. Electrical measurements

Dark current and steady-state photocurrent measurements were made using a Keithley 485 auto-ranging picoammeter and low-noise DC supply. Light sources were LEDs of the required wavelength, coupled to the sample via the quartz rod. The light output from the rod was calibrated versus LED current prior to use. For switch-on/switch-off measurements, the LED was driven from the 50 ohm output of a Thurlby Thandar TG1304 function generator, via a series resistor to set the desired current. For TPC measurements, shorter current pulses (0.1 to 1 μs) at up to 2 A were provided using a Renesas EL7104 laser driver IC. Photocurrents were pre-amplified, recorded on a Tektronix 3052 DSO and transferred to a PC for analysis.

In the TPC experiment, 4 to 6 time segments spanning from microseconds to seconds were edited into one logarithmically-spaced photocurrent decay curve, used to calculate the density of localised states (DOS) versus energy via a Fourier-transform technique [6, 7].

3. Results and discussion

3.1. Dark current activation

An Arrhenius plot of dark conductivity vs. reciprocal absolute temperature is shown in figure 2. The graph divides broadly into: (i) a higher temperature region (260-350 K) of activation energy 0.7 eV, (ii) a lower temperature region (160-180 K) of activation energy 0.2 eV, (iii) a curved intermediate region (180-260 K), with no single activation energy. Region (i) may be attributed unambiguously to thermal band-to-band (intrinsic) kinetics. The activation energy is roughly half the bandgap energy of 1.5 eV, as expected [7]. Region (ii) suggests extrinsic behaviour, with conduction

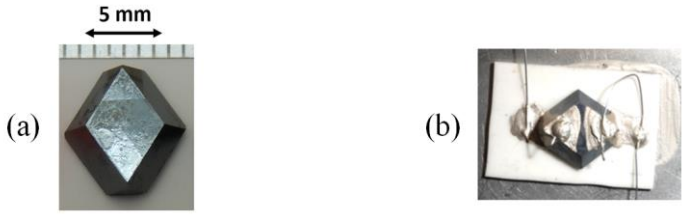

Figure 1. (a) MAPI crystal approximately 2 mm thick following three growth stages, (b) MAPI crystal with silver paste contacts, mounted on ceramic substrate.

taking place via a different thermally activated process. This might involve transport via surface channels or interlinked structural defects within the crystal bulk, which we have yet to investigate. The intermediate region (iii) would then represent a transition from (inhomogeneous) current flow via extrinsic processes at low temperatures, where the bulk crystal is largely insulating, through a mixed phase in which both intrinsic and extrinsic processes may be conjoined, to the intrinsic phase where the bulk crystal predominates. The measured dark conductivity of 4×10^{-8} S/cm at 300 K, with a variation between samples of around a factor of 2, lies within the range reported in the literature [8, 9].

Discontinuities in transport measurements with temperature, attributed to phase transitions in the perovskite crystal structure, have been reported [10]. These are known to occur at 165 K (orthorhombic to tetragonal) and 327 K (tetragonal to cubic). However, we observed no specific effects over the temperature range studied here. We thus conclude that the crystal remained in its tetragonal phase. We note however that small hysteresis [9] effects, dependent upon whether the sample current is measured moving from high to low temperature or vice-versa, are observed but do not substantially change the above reasoning.

3.2. Dark current-voltage curves

Dark current-voltage curves measured at temperatures of 298, 250 and 210 K are shown in figure 3. Below 3 V the I-V curve is substantially linear and shows the thermal activation discussed in section 3.1 above. However in the range 10-50 volts the curve deviates significantly from linear towards a power-law, of index 2 to 3. This behaviour has been reported previously for these materials [4, 5] and linked to the onset of space-charge limited currents (SCLC). The conditions for SCLC involve trap-filling, with the 'knee' representing the trap-filled voltage:

$$V_{TFL} = \frac{qn_{trap}L^2}{2\varepsilon_0\varepsilon_r} \quad (1)$$

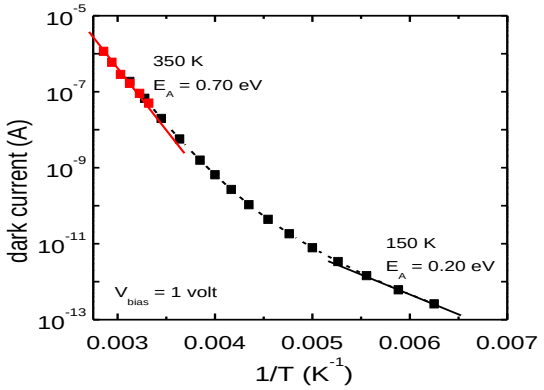

Figure 2. Arrhenius plot of dark current vs. reciprocal temperature.

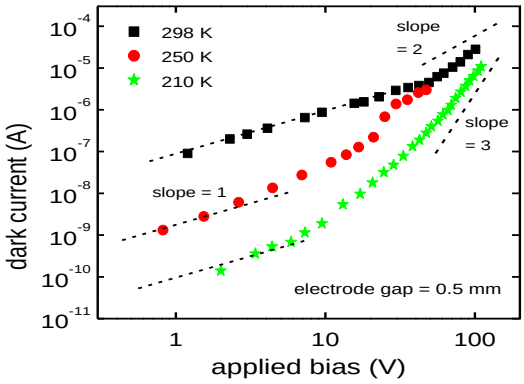

Figure 3. DC current-voltage curve measured at three different temperatures.

where n_{trap} is the trap density, L the conduction path length, ε_0 the permittivity of free space, ε_r the relative permittivity of the material and q the electronic charge. Setting L = 0.1 cm, n_{trap} = 10^{10} cm^{-3} and ε_r = 6 (the high frequency limit based on the refractive index) yields V_{TFL} = 15 V, in accordance with our observations. A trap density of 10^{10} cm^{-3} is remarkably low, on a par with the best inorganic semiconductor samples. However, recent investigations of the dielectric properties of organic-inorganic lead halide perovskites [11] has revealed their remarkably high value of low-frequency relative permittivity, of order 10^4 in the range 10 mHz-1 Hz corresponding to the timescale of the above experiment. Adopting this value, the trap density would be of order 10^{14} cm^{-3}, still a low figure, more in keeping with multicrystalline and thin-film semiconductors.

3.3. Steady-state and switch-on/switch-off photocurrent

The room-temperature steady-state photocurrent versus photon flux at 650 nm and 830 nm plotted on a log-log scale is shown in figure 4. Both curves bear a similar form, but differ somewhat in detail. Below 10^{15} cm^{-2} s^{-1}, photocurrent is roughly linearly dependent on photon flux. Above this value, the photocurrent increases less steeply and follows a square-root dependence. These two regions strongly suggest two different recombination mechanisms. A close to linear dependence suggests recombination via bandgap states, while square-root dependence at higher generation rates in direct-gap materials is characteristic of bimolecular recombination [12]. Although the behaviour at both wavelengths is quite similar, there are minor differences which may be attributed to the smaller optical absorption depth of around 1 µm at 650 nm, compared with 10 to 100 µm at 830 nm which lies on the MAPI optical absorption edge [13]. This will give rise to a greater carrier density close to the surface in the former case, resulting in earlier onset of bimolecular recombination.

The photocurrent overshoot (and undershoot) observed on application and removal of light shown in figure 5 is typical of a variety of longer time-scale phenomena reported for bulk MAPI samples and solar cells, which may involve ionic redistribution [14]. This exemplifies the challenges encountered when measuring and interpreting carrier transport in these materials. It should be noted that the data in figure 4 were recorded after allowing the current to stabilise.

3.4. Transient photocurrent spectroscopy

Transient photocurrent decays over a range of temperatures from 140 K to 270 K are shown in figure 6. There are a number of features (changes in gradient) in the decays, which are likely associated with carrier trapping and emission kinetics between band (transport) states and localised gap states. In order to identify these states we have applied DOS spectroscopy [6, 7], with the results shown in figure 7 on a log scale and in figure 8 on a linear scale. These plots emphasise different aspects of the DOS. With reference to figure 7, a reasonably consistent overlap of the DOS curves at deeper energies is obtained

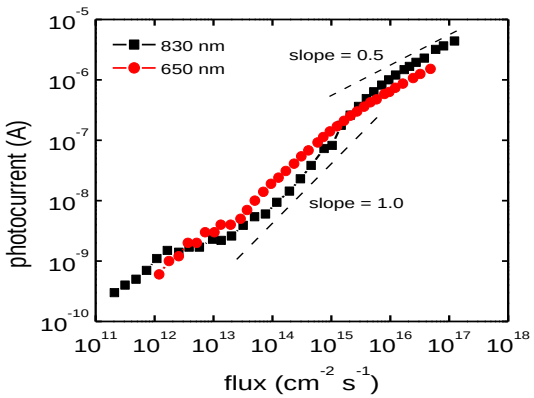

Figure 4. Steady-state photocurrent vs. photon flux at 650 nm and 830 nm.

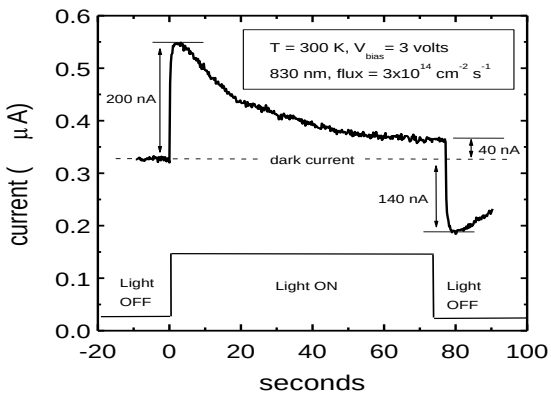

Figure 5. Photocurrent overshoot and undershoot relative to dark current.

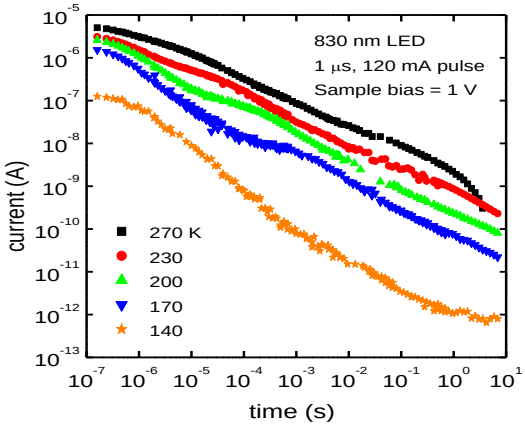

Figure 6. Transient photocurrent decays between 140 K and 270 K.

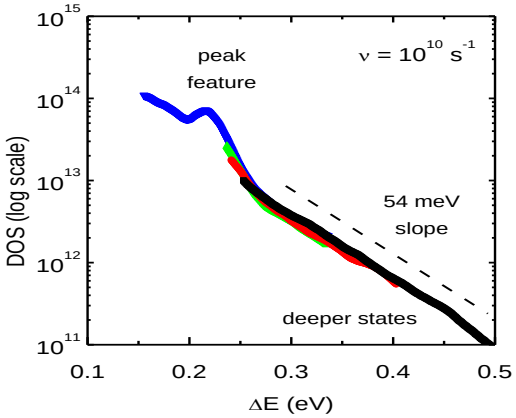

Figure 7. DOS on a log scale vs. energy from band edge ΔE. An attempt to escape frequency of 10^{10} s^{-1} gives optimal fit for deeper states.

by adopting an attempt to escape frequency of 10^{10} s^{-1}. This parameter essentially defines the energy scale of the DOS relative to the band edge. The DOS follows a broadly exponential reduction with increasing energy, and a characteristic slope of 54 meV. However the absolute DOS scale (y-axis) is more difficult to quantify as it depends on several factors, such as carrier mobility, which has not been determined here. For simplicity, the DOS scale in figure 7 has been aligned broadly with our estimate for the localised state density obtained from SCLC (section 3.2). This figure is in keeping with more recent estimates of defect density in single crystal MAPI [15]. Figure 8 reveals the peak 'feature' evident in figure 7 more clearly. It can be observed that the attempt to escape frequency shifts the peak along the energy axis by an amount dependent on the experimental temperature – ideally there will be a single frequency at which all coincide. The optimum overlap occurs at 10^{11} s^{-1}, with a corresponding peak energy $\Delta E_P = 0.26$ eV.

It should be noted that the TPC method applied to a planar sample is unable to distinguish *a priori* between electron and hole transport, and thus the above procedure may be sensitive to (empty) states above the Fermi level, or to (filled) states below it, frequently depending upon whether electrons or holes, respectively, are the majority carrier. As carrier mobilities in MAPI single crystals [16] do not consistently favour either electrons or holes, we cannot state here with any authority which half of the bandgap is being probed by TPC.

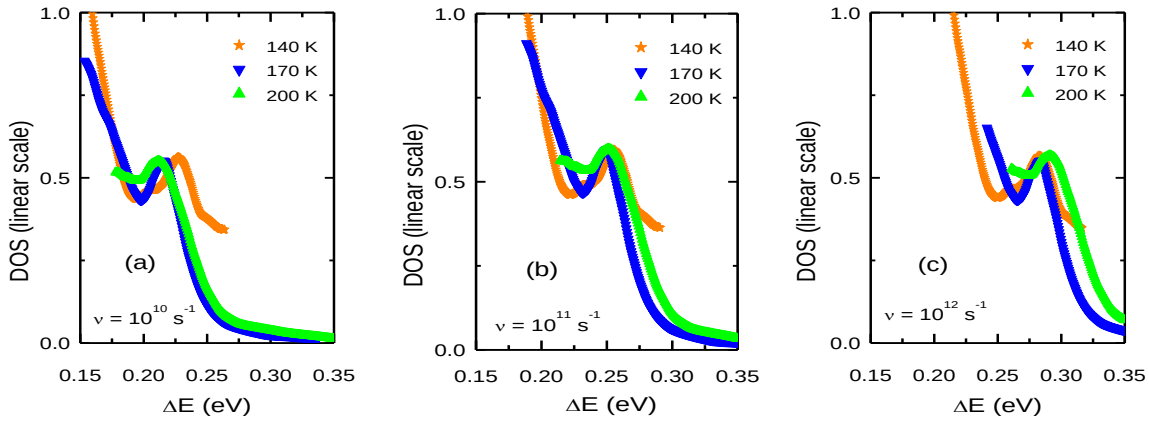

Figure 8. DOS on a linear scale vs. energy from band edge ΔE. An attempt to escape frequency of 10^{11} s^{-1} (graph b) gives optimal fit for the peak feature, at energy $\Delta E_P = 0.26$ eV.

4. Conclusions

We have investigated the electronic transport properties of methylammonium lead tri-iodide single crystals grown by the inverse temperature crystallisation method. Our dark current measurements show similar room-temperature conductivity (4×10^{-8} S/cm), thermal activation energy (0.70 eV) and space-charge limited current behaviour as reported previously in the literature. Steady-state and transient photoconductivity measurements have been applied to investigate carrier interactions with localised states. The steady-state measurements are consistent with trap-mediated recombination below a flux of 10^{15} $cm^{-2}s^{-1}$, and bimolecular band-to-band recombination above this level. Some small wavelength-dependent variations occur, which probably reflect the higher volume generation rates that occur with more strongly absorbed light. Transient photoconductivity decays are consistent with multiple trapping in a narrow band of states 0.26 eV below the band edge with an attempt to escape frequency of 10^{11} s^{-1}, plus a broader exponential distribution of deeper states, of slope 54 meV. We are presently unable to say whether these states lie in the upper or the lower half of the bandgap. More generally, photoconductivity measurements display a rich variety of behaviour, unlikely to be adequately explained in terms of a 'stationary' model. In common with other more comprehensive studies, we conclude that (reversible) ionic migration or redistribution takes place on application and removal of electric fields or carrier concentration gradients. The resulting modified potential landscape will in turn influence electronic carrier transport; some outcomes may be beneficial, for example increasing effective carrier diffusion lengths, but others may be less desirable, since transport properties will be synchronised to the long timescales dictated by the landscape response.

Acknowledgments

The authors are grateful to S Anthony and C Moore for technical assistance, and to C Main for the legacy of his DOS spectroscopy software. The SC-Simul simulation software (University of Oldenburg) was used to visualise and explore certain density of states distributions.

References

[1] Green M A, Hishikawa Y, Dunlop E D, Levi D H, Hohl-Ebinger J and Ho-Baillie A W Y 2018 *Prog. Photovolt. Res. Appl.* **26** 427
[2] Green M A and Ho-Baillie A 2017 *ACS Energy Lett.* **2** 822
[3] Wang D, Wright M, Elumalai N K and Uddim A 2016 *Sol. Energy Mater. Sol. Cells* **147** 255
[4] Saidaminov M I *et al* 2015 *Nat. Commun.* **6** 7586
[5] Liu Y *et al* 2015 *Adv. Mater.* **27** 5176
[6] Main C, Brüggemann R, Webb D P and Reynolds S 1992 *Sol. St. Commun.* **83** 40
[7] Main C 1997 *MRS Symp. Proc.* **467** 167
[8] Sveinbjörnsson K, Aitola K, Zhang X, Pazoki M, Hagfeldt A, Boschloo G and Johansson E M J 2015 *J. Phys. Chem. Lett.* **6** 4259
[9] Khenkin M V, Amasev D V, Kozyukhin S A, Sadovnikov A V, Katz E A and Kazanskii A G 2017 *Appl. Phys. Lett.* **110** 222107
[10] Li D, Wang G, Cheng H-C, Chen C-Y, Wu H, Liu Y, Huang Y and Duan X 2016 *Nat. Commun.* **7** 11330
[11] Slonopas A, Kaur B and Norris P 2017 *Appl. Phys. Lett.* **110** 222905
[12] Bube R H 1992 *Photoelectronic Properties of Semiconductors* (Cambridge: Cambridge University Press)
[13] De Wolf S, Holovsky J, Moon S-J, Löper P, Niesen B, Ledinsky M, Haug F-J, Yum J-H and Ballif C 2014 *J. Phys. Chem. Lett.* **5** 1035
[14] Eames C, Frost J M, Barnes P R F, O'Regan B C, Walsh A and Islam M S 2015 *Nat. Commun.* **6** 7497
[15] Wenger B, Nayak P B, Wen X, Kesava S V, Noel N K and Snaith H 2017 *Nat. Commun.* 8 590
[16] Herz L 2017 *ACS Energy Lett.* **2** 1539